RESEARCH ARTICLE
SPACE PHYSICS: MAGNETOSPHERIC PHYSICS

Earth and Planetary Physics
6: 465–473, 2022
doi: 10.26464/epp2022041

Observations of kinetic Alfvén waves and associated electron acceleration in the plasma sheet boundary layer

ZeHao Zhang, ZhiGang Yuan*, ShiYong Huang, XiongDong Yu, ZuXiang Xue, Dan Deng, and Zheng Huang

School of Electronic Information, Wuhan University, Wuhan 430072, China

Key Points:

- The Magnetospheric Multiscale (MMS) Mission observed strong kinetic Alfvén waves (KAWs) carrying a parallel disturbed electric field with an amplitude up to 8 mV/m in the plasma sheet boundary layer (PSBL).
- The KAWs became more electrostatic-like and filled with high-frequency ion acoustic waves during electron acceleration.
- These results provide direct evidence of electron acceleration by KAWs embodying electrostatic ion acoustic waves in the PSBL.

Citation: Zhang, Z. H., Yuan, Z. G., Huang, S. Y., Yu, X. D., Xue, Z. X., Deng, D., and Huang, Z. (2022). Observations of kinetic Alfvén waves and associated electron acceleration in the plasma sheet boundary layer. *Earth Planet. Phys.*, *6*(5), 465–473. http://doi.org/10.26464/epp2022041

Abstract: Kinetic Alfvén waves (KAWs), with a strong parallel disturbed electric field, play an important role in energy transport and particle acceleration in the magnetotail. On the basis of high-resolution observations of the Magnetospheric Multiscale (MMS) Mission, we present a detailed description of the acceleration process of electrons by KAWs in the plasma sheet boundary layer (PSBL). The MMS observed strong electromagnetic disturbances carrying a parallel disturbed electric field with an amplitude of up to 8 mV/m. The measured ratio of the electric to magnetic field perturbations was larger than the local Alfvén speed and was enhanced as the frequency increased, consistent with the theoretical predictions for KAWs. This evidence indicates that the electromagnetic disturbances should be identified as KAWs. During the KAWs, the energy flux of electrons at energies above 1 keV in the parallel and anti-parallel directions are significantly enhanced, implying occurrences of electron beams at higher energies. Additionally, the KAWs became more electrostatic-like and filled with high-frequency ion acoustic waves. The energy enhancement of electron beams is in accordance with the derived work done with the observed parallel disturbed electric field of KAWs, indicating electron acceleration caused by KAWs. Therefore, these results provide direct evidence of electron acceleration by KAWs embodying electrostatic ion acoustic waves in the PSBL.

Keywords: kinetic Alfvén wave; plasma sheet boundary layer; electron energization; Poynting flux

1. Introduction

An outstanding problem in magnetospheric physics is the nature of the energy transfer process by which the energy stored in the magnetotail is transferred into the Earth's ionosphere and ultimately is deposited in the low-altitude atmosphere (Wygant et al., 2002; Yuan ZG et al., 2007; Fu HS et al., 2011; Chen CX and Wang CP, 2019; Chen CX, 2021). The wave–particle interaction is considered an important candidate for energy conversion. Although studies of wave–particle interaction in magnetospheric dynamics have made great progress, some open problems still exist (Huang SY et al., 2015). With advances in observation equipment, satellites can observe magnetic and electric fields, as well as particles, with high time or energy resolution. This enables us to study the processes of wave–particle interactions in the Earth's magnetotail in detail, in particular for waves in the ion cyclotron frequency range, such as electromagnetic ion cyclotron waves (Kennel and Petschek, 1966; Gomberoff and Elgueta, 1991; Fu HS et al., 2014; Wang XY et al., 2017) and Alfvén waves (Keiling et al., 2005; Chen L et al., 2013).

Alfvén waves are a kind of magnetohydrodynamic electromagnetic waves that propagate in magnetized plasma at a frequency lower than the local proton cyclotron frequency. After the kinetic effects of the particles on the dispersion relation are considered, Alfvén waves are coupled with some electrostatic waves and become quasi-electrostatic waves. In hot plasma, the shear Alfvén waves are coupled with ion acoustic waves to form kinetic Alfvén waves (KAWs; Lysak and Lotko, 1996; He JS et al., 2012a). For KAWs, the wavelength in the direction of the background magnetic field can be larger than that perpendicular to the background magnetic field equivalent to the ion cyclotron radius ($\lambda_{//} \gg \lambda_{\perp} \propto \rho_i$, where ρ_i is the ion gyroradius; Hollweg et al., 1999; Cramer et al., 2001; Voitenko and Goossens, 2006; He JS et al., 2012b). Unlike Alfvén waves, one of the important characteristics of KAWs is a disturbed electric field component parallel to the direction of the wave vector owing to acoustic effects. In addition, the ratio of electric to magnetic field perturbations of KAWs is larger than the local Alfvén speed and is enhanced with an increase in frequency (Wygant et al., 2002; Moya et al., 2015; Huang HT et al., 2018).

Correspondence to: Z. G. Yuan, y_zgang@vip.163.com
Received 03 MAY 2022; Accepted 19 MAY 2022.
Accepted article online 15 JUL 2022.

Because KAWs can carry a significant Poynting flux and a strong parallel electric field (Moya et al., 2015), the Poynting flux of KAWs has been proposed as a possible energy source to accelerate particles (Kletzing, 1994) and as the source of auroras (Angelopoulos et al., 2002; Keiling et al., 2003; Keiling, 2009; Duan SP et al., 2012, 2016). Kinetic Alfvén waves can resonate with electrons so as to accelerate or heat the electrons (Moya et al., 2015). Observations suggest that KAWs play an important role in the heating of ions (Chaston el al., 2014), the acceleration of electrons in the plasma sheet boundary layer (PSBL; Chaston et al., 2006; Duan SP et al., 2012), and the generation of field-aligned electrons and parallel heating of electrons (Wygant et al., 2002).

Previous studies have shown KAWs in magnetotail reconnection regions, the plasma sheet, and the PSBL, with observations by Polar spacecraft, Cluster satellites, and other satellites (Wygant et al., 2002; Chaston et al., 2005, 2009; Dombeck et al., 2005; Yuan ZG et al., 2007; Dai L, 2009; Duan SP et al., 2012, 2016; Dai L et al., 2017). The most energetic KAWs have been found in the PSBL (Keiling et al., 2005). In previous studies, some satellites were unable to provide three-dimensional (3-D) electric fields because the electric field in the direction of spin could not be directly measured and had to be calculated under certain conditions (Yuan ZG et al., 2007). Furthermore, the low time or energy resolutions of the observed electron energy spectrum made it difficult to display the electron acceleration by KAWs in detail. Compared with previous satellites, the MMS has extremely high resolution data for the 3-D magnetic and electric fields. The sampling frequencies of the magnetic and electric fields are 128 Hz and 8,192 Hz, respectively (Ergun et al., 2016; Lindqvist et al., 2016; Russell et al., 2016). In particular, the time resolutions are 30 ms and 150 ms to measure the electron and ion distribution functions (Pollock et al., 2016; Young et al., 2016), respectively. In this study, we present a detailed description of MMS observations of KAWs in the PSBL on 31 May 2017. We used high-resolution data of the 3-D electric and magnetic fields from the MMS satellite to calculate the power spectral densities (PSD) of the electric and magnetic fields so as to identify KAWs. Similarly, we obtained the electron two-dimensional (2-D) velocity space distribution function with a high time resolution before and during KAWs, to observe the process of electron acceleration by KAWs in detail.

2. Observations

This event was observed by the MMS satellite between 07:21:20 and 07:22:10 universal time (UT) on 31 May 2017. In the geocentric solar ecliptic (GSE) coordinate system, the MMS is located at (−20, −14, 4)R_E (R_E is the Earth radius) of Earth's magnetotail.

2.1 Kinetic Alfvén Wave Observations

The PSBL is a boundary layer between the lobe and the central plasma sheet. Figure 1 shows the plasma and magnetic fields observed by the MMS. The plasma temperature in the PSBL was higher than that in the lobe region, whereas the ion β_i (the ratio of the ion thermal pressure to the magnetic pressure) was between 0.3 and 0.5 in the PSBL (Baumjohann et al., 1988). During the time interval denoted by the two black vertical dashed lines in Figure 1, from 07:21:37 to 07:21:52 UT, the total magnetic field (Figure 1a) showed a declining tread, both the ion velocity and temperature (Figures 1b–1e) increased significantly, and the plasma β_i (Figure 1g) reached the criterion of the PSBL (Huang SY et al., 2020), implying that the spacecraft left the lobe and entered the PSBL.

Figure 2 shows the electric and magnetic fields, as well as the energy spectrum of electrons and ions observed by the MMS. After subtracting the background component from the observed magnetic field (Figure 2a) in all three directions in the GSE coordinate system, we were able to obtain the disturbances of the magnetic field (δB_x, δB_y, δB_z), which are shown in Figure 2b. This result shows that obvious magnetic field perturbations are present in all three directions. Perturbations of the electric field (δE_x, δE_y, δE_z) could also be obtained following the same procedure. As shown in Figure 2d, intense electric field perturbations appeared and the magnitude of δE_x was up to 8 mV/m at 07:21:46 UT. Figure 2c shows a parallel magnetic field and two perpendicular magnetic fields. Like Figure 2c, Figure 2e shows a strong parallel electric field with an amplitude of up to 8 mV/m in the field-aligned coordinates around 07:21:46 UT as well as two perpendicular electric fields. Figure 2f shows three components of the Poynting flux calculated by δE and δB. Figure 2g presents the total Poynting flux (S_t) and the parallel Poynting flux ($S_{//}$; the positive means propagating along the field-aligned direction). The most important characteristics of KAWs are the strong parallel electric field and the Poynting flux. The Poynting flux of KAWs is parallel to the magnetic field, very similar to shear Alfvén waves, which is a characteristic of the KAW eigenmode confined by the plasma sheet (Duan SP et al., 2016). According to the above-mentioned observations, the parallel disturbed electric field and the Poynting flux reached 8 mV/m and 10 μW/m^2, respectively. As shown in Figure 2g, the field-aligned component of the Poynting flux $S_{//}$ dominated and accounted for 95% of the total Poynting flux S_t. Therefore, those observations imply that these disturbances are KAWs propagating in the field-aligned direction. Figure 2h and 2i display electron and ion fluxes, respectively. As shown in Figure 2h, electron fluxes above 1 keV were significantly enhanced within the two black vertical dashed lines, which is discussed in Section 2.2. As shown in Figure 2i, the ion fluxes were enhanced for <1 keV before 07:21:40 UT, whereas they increased by several kiloelectron volts after 07:21:40 UT, implying the spacecraft left the lobe and entered the PSBL.

For KAWs associated with intense electric and magnetic field perturbations, the ratio of electric to magnetic field perturbations should be larger than the local Alfvén speed (Gary, 1986; Hollweg, 1999; Voitenko and Goossens, 2006). We performed a wavelet analysis to compute the PSD of the magnetic and electric fields during the KAWs between 07:21:44 and 07:21:50 UT (denoted by the two black vertical dashed lines in Figure 2), which are shown in Figures 3a and 3b, respectively. In the frequency range denoted by the left two vertical dashed lines in Figure 3a–3b, the PSD for the parallel and perpendicular components of both the magnetic and electric fields are obviously enhanced, implying that the KAWs have frequencies below the local ion frequency, denoted by the vertical solid line. Figure 3c shows the ratio of $(\delta E_\perp/\delta B_\perp)/V_A$ (where $\delta E_\perp$ and $\delta B_\perp$ correspond to the absolute values of the

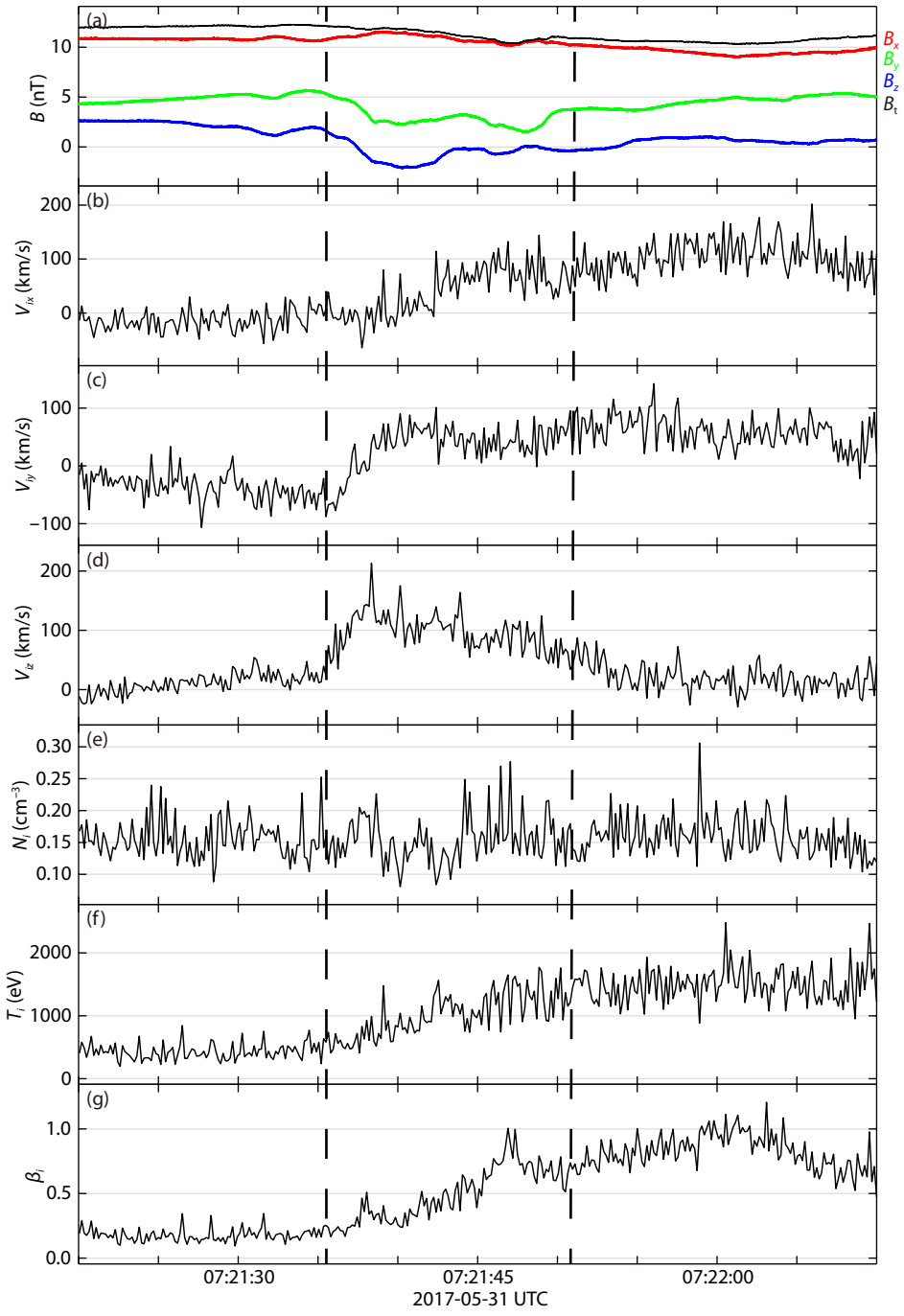

Figure 1. Plasma and magnetic fields observed by Magnetospheric Multiscale (MMS) Mission 1 during crossing of the plasma sheet boundary layer. (a) Three components and magnitudes of the magnetic field. (b–d) Three components of the ion velocity in geocentric solar ecliptic coordinates. (e–f) Ion density and temperature. (g) Ion β_i (ratio of ion thermal pressure to magnetic pressure).

perpendicular disturbed electric and magnetic field amplitudes and V_A is the local Alfvén speed) and the theoretical prediction. The theoretical prediction is calculated by combining the dispersion relation of KAWs, $\omega^2 = k_{//}^2 V_A^2 \left(1 + k_\perp^2 \rho_i^2\right)$ (Lysak and Lotko, 1996; Lysak, 1998), and the polarization properties of KAWs in the low frequency limit ($\omega \ll \omega_i$) warm plasma, $\dfrac{\delta E_\perp}{\delta B_\perp} = \dfrac{V_A(1 + k_\perp^2 \rho_i^2)}{\sqrt{1 + k_\perp^2(\rho_i^2 + \rho_s^2)}}$ (where ω_i is the ion cyclotron frequency, $k_{//}$ is the parallel component of the wave vector, $k_\perp$ is the transverse component of the wave vector, and ρ_s is the ion acoustic gyroradius; Stasiewicz et al., 2000; Chaston et al., 2012). In the rest of the reference frame, KAWs have frequencies that are less than the ion cyclotron frequency ω_i, whereas the plasma flow speed exceeds 100 km/s during the interval denoted by the two black vertical dashed lines in Figure 1. Thus, consistent with other cases observed in the PSBL (Chaston et al., 2012), we expected that in the spacecraft frame, all the spectrum properties would be dominated by the Doppler shift, i.e., $\omega_{sc} = 2\pi f_{sc} = \omega + k \cdot v_f \gg \omega$ (where v_f is the plasma flow speed and ω_{sc} and ω are the frequencies in the satellite and plasma

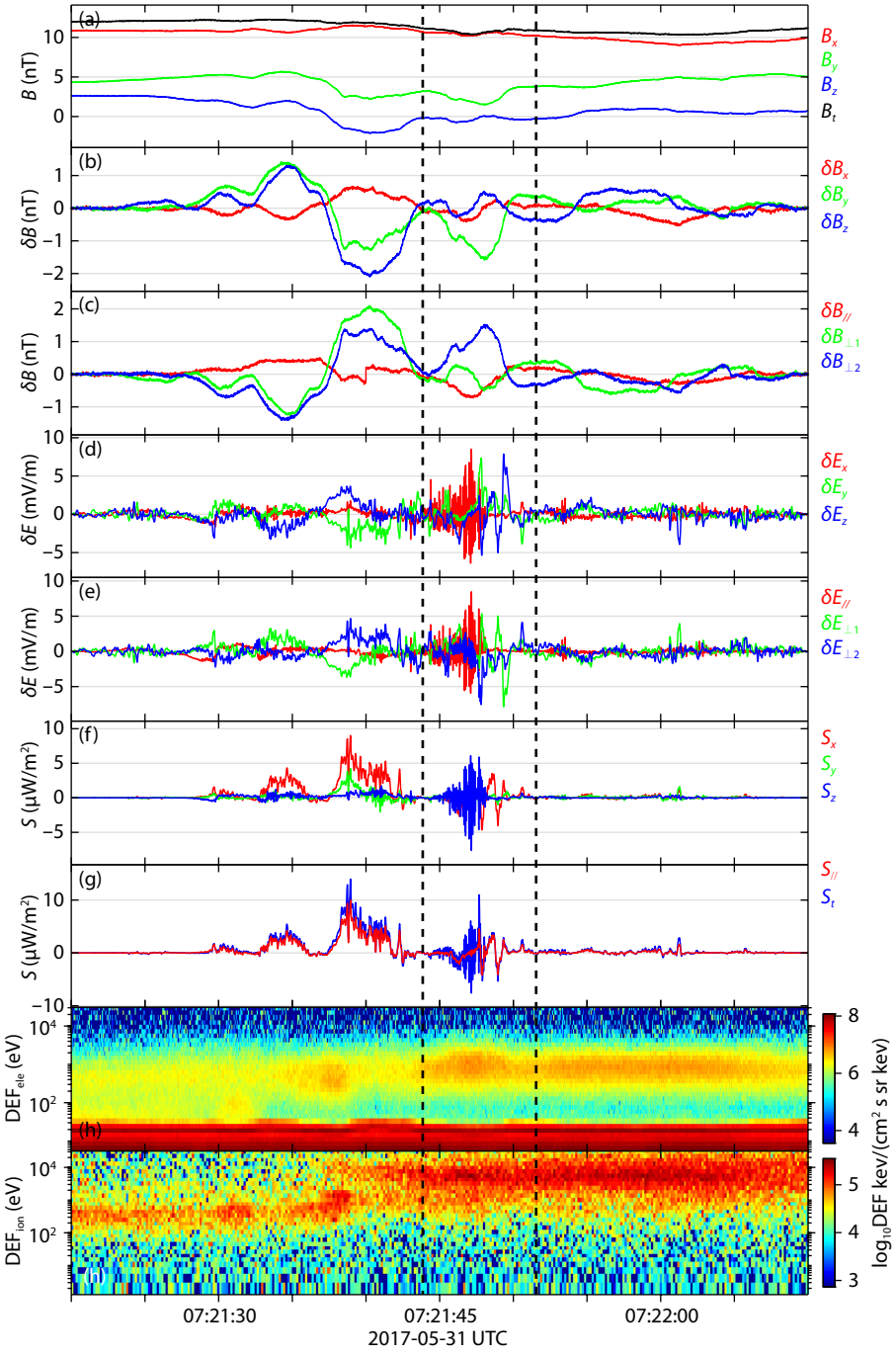

Figure 2. Magnetic and electric fields, and the electron and ion differential energy flux (DEF) during kinetic Alfvén waves observed by MMS1. (a) Observed magnetic field. (b) Three components of magnetic field perturbations. (c) Parallel magnetic field and two perpendicular magnetic fields. (d) Three components of the electric field perturbations. (e) Parallel electric field and two perpendicular electric fields. (f) Three components of the Poynting flux. (g) Parallel Poynting flux (red) and total Poynting flux (blue). (h–i) Electron and ion DEF.

frames, respectively, $\omega_{sc} = 2\pi f_{sc}$). The propagation angle of the KAW is estimated at approximately 23° by the Minimum Variance Analysis (MVA, Sonnerup and Scheible, 1998). In the frequency range denoted by the left two vertical black dashed lines, as shown in Figure 3c, the ratio of $\delta E_\perp/\delta B_\perp$ is larger than the local Alfvén speed and is enhanced as the frequency increases, consistent with the theoretical predictions for KAWs (Wygant et al., 2002; Chaston et al., 2014; Moya et al., 2015). Note that in the frequency range denoted by the right two vertical red dashed lines, as shown in Figure 3, the PSDs of the parallel disturbed electric field are obviously enhanced and exceed those of the perpendicular disturbed electric field, whereas the disturbed magnetic field remains at a low level, implying that the high-frequency emission is electrostatic-like.

2.2 Parallel Electron Energization

Kinetic Alfvén waves can heat and accelerate charged particles effectively (Kletzing, 1994; Wygant et al., 2002; Duan SP et al.,

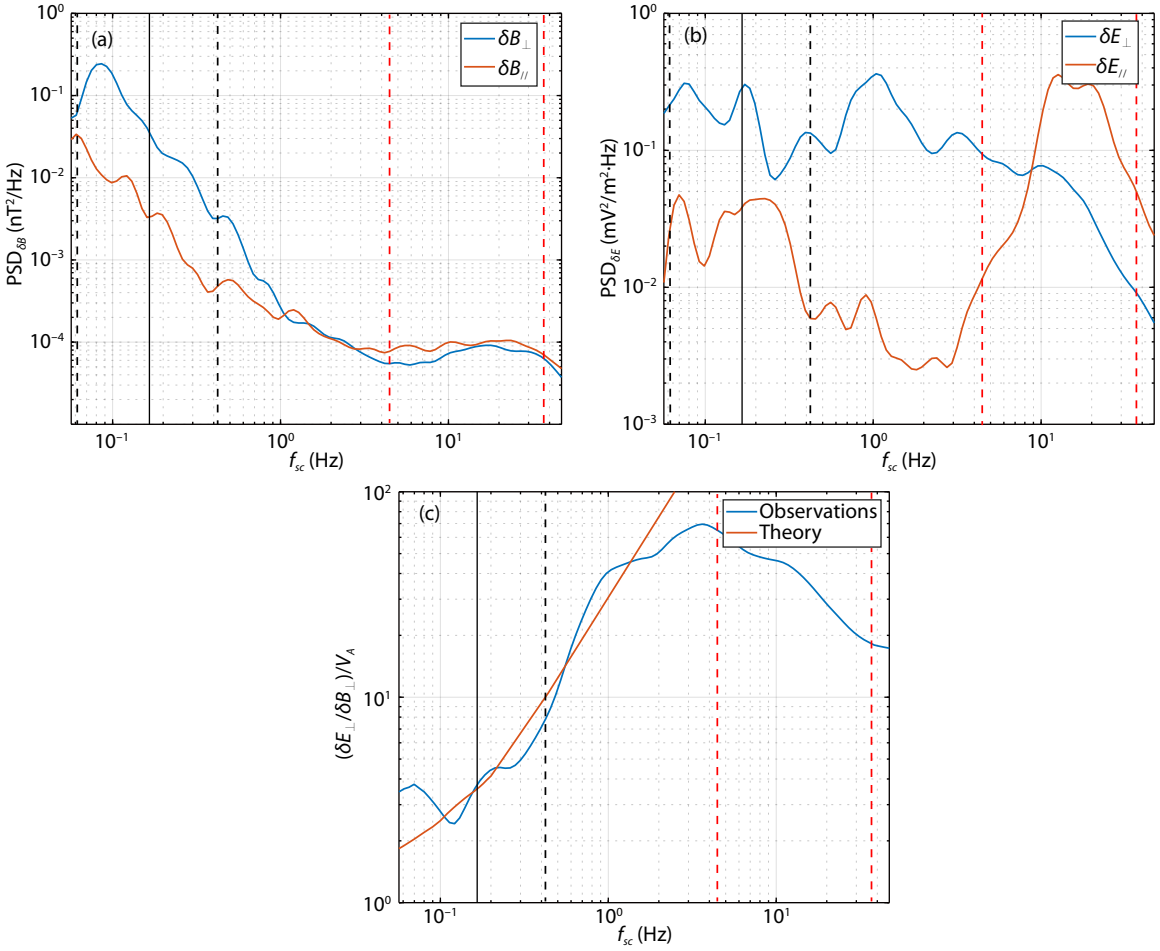

Figure 3. (a) Wavelet power spectral densities (PSD) of parallel magnetic fields (red) and perpendicular magnetic fields (blue). (b) Wavelet PSD of parallel electric fields (red) and perpendicular electric fields (blue). (c) Ratio of perpendicular electric to magnetic field divided by the local Alfvén speed (blue) and the theoretical prediction (red). The black vertical solid line denotes the local proton cyclotron frequency. The left two black vertical dashed lines denote the frequency range of kinetic Alfvén waves. The right two red vertical dashed lines denote the frequency range of electrostatic ion acoustic waves.

2016). As shown in Figure 2g, the energy flux of electrons is enhanced during KAWs, suggesting parallel electron energization by the KAWs. In the following content, we focus in detail on the process of electron acceleration by KAWs.

Figure 4 shows the parallel electric fields and the pitch angle distribution of electron fluxes at energies of 0.05–3.8 keV. During the interval of 07:21:44–07:21:50 UT, denoted by the two black vertical dashed lines in Figure 4, the pitch angle distribution of electron fluxes appears to be enhanced in the parallel and anti-parallel directions, especially for the higher energies of 1.4–2.9 keV (Figures 4g–4i). This enhancement is accompanied by the strong parallel electric field and strong Poynting flux shown in Figures 4a and 2g. The enhancement of electron energy fluxes at energies above 1 keV shown in Figure 2h can be explained by enhancements of the electron fluxes in the parallel and anti-parallel directions, as shown in Figures 4e–4i. The electron flux distribution for energies above 1 keV in the parallel and anti-parallel directions can be produced by the parallel electric fields of KAWs.

Figure 5 shows the 2-D velocity space distribution of electrons in two directions of $V_{//}$, $V_{\perp 1}$ and $V_{\perp 2}$. Here $V_{//}$, $V_{\perp 1}$ and $V_{\perp 2}$ are parallel and two perpendicular components of the velocity in the field-aligned coordinates. For each distribution map, the accumulation time length is 0.3 s. As denoted by the three arrows in Figure 4, we selected three time periods before and during KAWs in the PSBL to discover the details of electron acceleration by KAWs. At the beginning, as shown in the left and middle panels of Figure 5a, electrons have an almost isotropic distribution plus two beams in the parallel and anti-parallel directions before the KAWs. Those two beams have $V_{//}$ of about 10×10^3 km/s or -10×10^3 km/s, corresponding to an energy of ~0.28 keV. Unlike Figure 5a, the left and middle panels of Figures 5b–5c show strong anisotropic distributions with obvious parallel extents to high velocities for $|V_{//}| > 10 \times 10^3$ km/s during KAWs, implying parallel or anti-parallel electron beams at energies >0.28 keV. Especially as shown in Figure 5c, during the strongest KAWs, electron fluxes of parallel or anti-parallel electron beams for $|V_{//}| > 20 \times 10^3$ km/s (energies >1.1 keV) obviously increase, which is in accordance with enhancements of electron fluxes in the parallel and anti-parallel directions at energies of 1.4–2.9 keV shown in Figures 4g–4i.

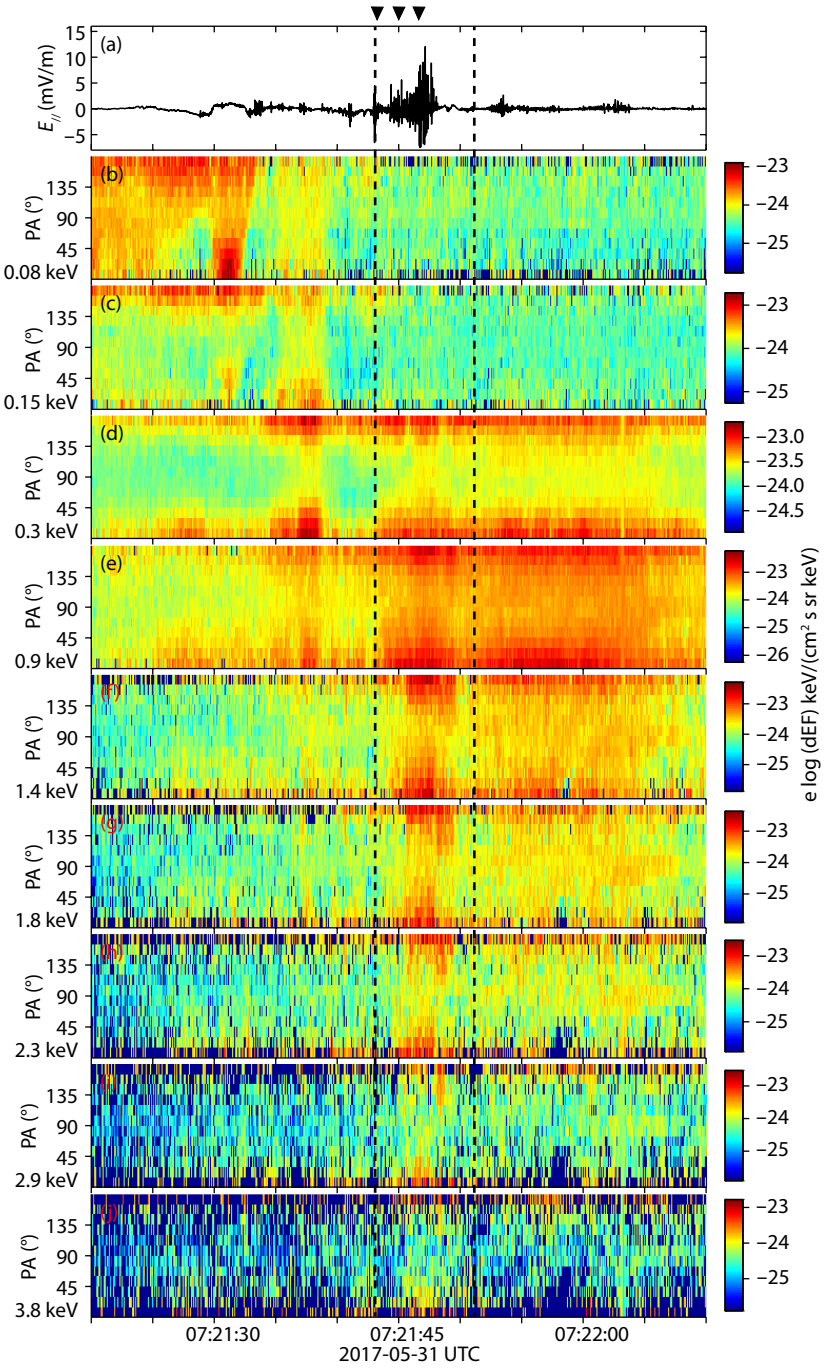

Figure 4. Parallel disturbed electric field ($E_{//}$) and pitch angle (PA) distribution of electron differential energy fluxes (DEF) at energies of 0.08–3.8 keV.

3. Discussion and Conclusions

We present detailed MMS observations of KAWs in the PSBL on 31 May 2017. The observations of strong parallel electric fields and the Poynting flux coincide with previous results (Wygant et al., 2002; Dombeck et al., 2005; Duan SP et al., 2016, 2017). Furthermore, the parallel component of the Poynting flux accounts for 95% of the total Poynting flux, and the electric field in the parallel direction reaches 8 mV/m. By PSD analysis of the electric and magnetic field disturbances, we demonstrated that the frequency of KAWs is below the ion cyclotron frequency, whereas the ratio of $(\delta E/\delta B)/V_A$ is enhanced as the frequency increases and is consistent with the calculated theoretical predictions. Among the three components of the disturbed electric field, the parallel electric fields carried by KAWs are very strong. Using the parallel electric fields, we were able to calculate the efficiency with which the KAWs accelerated electrons. On the basis of the solution of the coupled Maxwell–Vlasov equations, the scale sizes and perpendicular and parallel potential drops for KAWs could be theoretically derived (Lysak and Lotko, 1996; Lysak, 1998). With observations of the MMS during KAWs from 07:21:44 to 07:21:50 UT, denoted by the two black vertical dashed lines in Figure 4, we could obtain the values of plasma parameters and waves. As a result, $T_i/T_e = 2.6$,

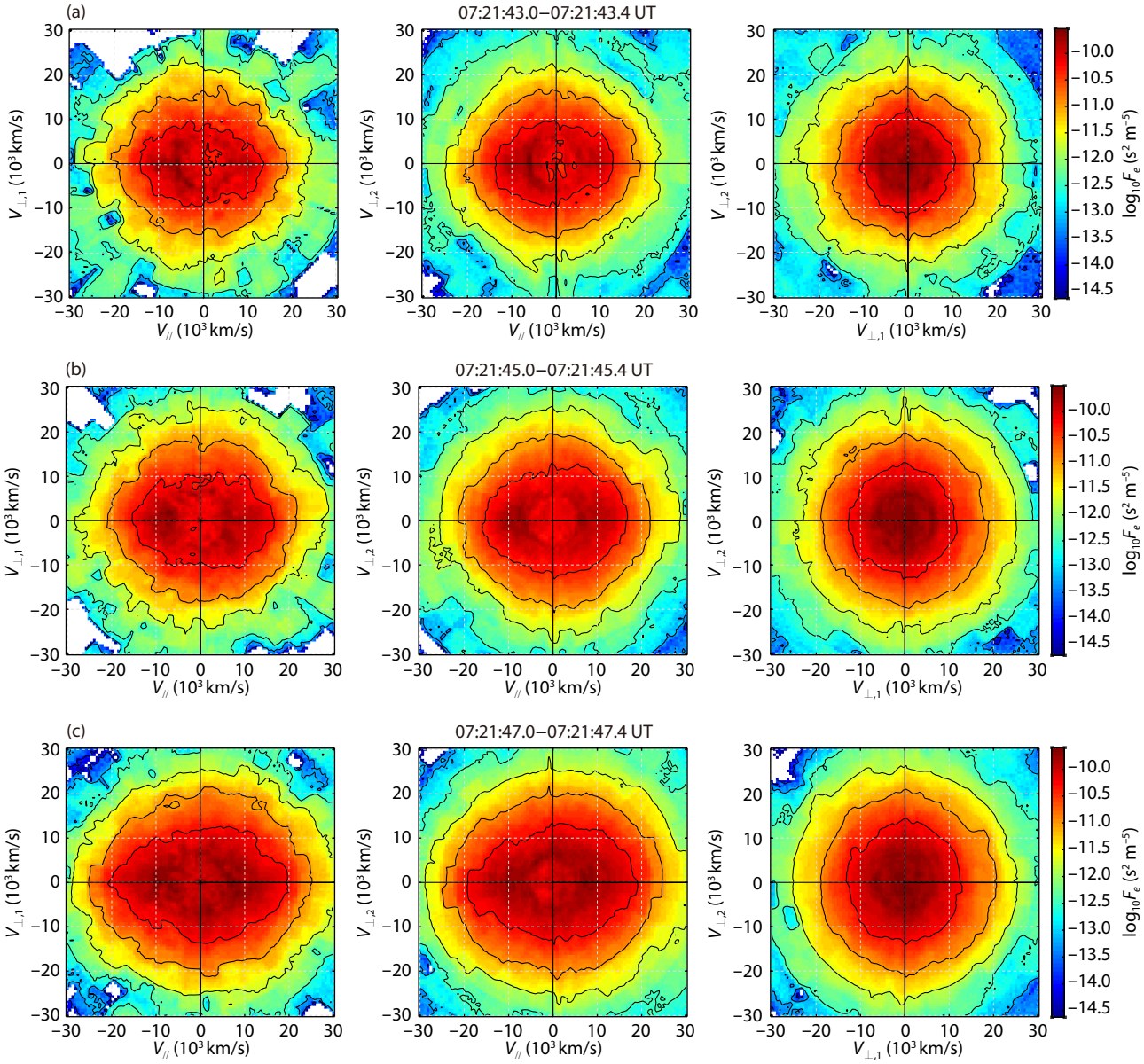

Figure 5. Electron two-dimensional velocity space distribution in parallel and two perpendicular to the magnetic field for three periods before and during kinetic Alfvén waves (KAWs), denoted by the three arrows in Figure 4. (a) Distribution before the KAWs. (b–c) Distributions during the KAWs.

$V_e/V_A = 10.2$, $c/\omega_{pe} = 1.87 \times 10^4$, $\delta E_{//} = 8$ mV/m, $\delta E_{//}/\delta E_{\perp} = 0.74$, and $(\delta E_{\perp}/\delta B_{\perp})/V_A = 3.8$, where c/ω_{pe} is the electron inertial length, c is the speed of light, ω_{pe} is the electron plasma frequency, and V_e is the electron thermal velocity. Finally, following the method of Lysak (1998), we estimated the parallel electric potential, $\delta\varphi_{//} \sim \lambda_{//}\delta E_{//}$, to 1.66 kV, where $\lambda_{//}$ is the wave length (or scale size) parallel to the background magnetic field. Therefore, the energy for the electron beam shown in Figure 5a could increase to 1.94 keV through work by the observed parallel electric field, which is consistent with the energy enhancement of the electron beam in Figure 4 and demonstrates that the electron beams at higher energies of 1.4–2.9 keV are a result of the acceleration by KAWs. By comparing the electron flux distributions at the pitch angles of 0° or 180° before and during KAWs, we could observe the process of electron acceleration by KAWs. At the same time, we presented a 2-D velocity space distribution function of electrons in parallel and two perpendicular directions. The electron distributions coincide with KAWs, indicating the process of electron acceleration.

In addition, during the interval of KAWs, denoted by the two black dashed lines in Figure 2, in the frequency range denoted by the right two red vertical dashed lines in Figure 3, the high-frequency emission was electrostatic with predominantly parallel polarization. The electrostatic emissions should be ion acoustic fluctuations as a result of evolution of the KAWs (Wahlund et al., 1994). These observations demonstrate that electrons are accelerated by the parallel electric field of KAWs embodying electrostatic ion acoustic waves in the PSBL. In conclusion, with observations of the MMS, this study provides direct evidence of electron acceleration by KAWs in the PSBL.

Acknowledgments

We acknowledge the entire MMS satellite team for providing such excellent data. The MMS observations are available via the Science Data Center at the Laboratory for Atmospheric and Space Physics at the University of Colorado Boulder (https://spdf.gsfc.nasa.gov/pub/data/mms/). This work is supported by the National Natural Science Foundation of China (Grant Nos. 41925018, 41874194).

References

Angelopoulos, V., Chapman, J. A., Mozer, F. S., Scudder, J. D., Russell, C. T., Tsuruda, K., Mukai, T., Hughes, T. J., and Yumoto, K. (2002). Plasma sheet electromagnetic power generation and its dissipation along auroral field lines. *J. Geophys. Res.*: *Space Phys.*, *107*(A8), 1181. https://doi.org/10.1029/2001JA900136

Baumjohann, W., Paschmann, G., Sckopke, N., Cattell, C. A., and Carlson, C. W. (1988). Average ion moments in the plasma sheet boundary layer. *J. Geophys. Res.*: *Space Phys.*, *93*(A10), 11507–11520. https://doi.org/10.1029/JA093iA10p11507

Chaston, C. C., Phan, T. D., Bonnell, J. W., Mozer, F. S., Acuña, M., Goldstein, M. L., Balogh, A., Andre, M., Reme, H., and Fazakerley, A. (2005). Drift-kinetic Alfvén waves observed near a reconnection X line in the earth's magnetopause. *Phys. Rev. Lett.*, *95*(6), 065002. https://doi.org/10.1103/PhysRevLett.95.065002

Chaston, C. C., Genot, V., Bonnell, J. W., Carlson, C. W., McFadden, J. P., Ergun, R. E., Strangeway, R. J., Lund, E. J., and Hwang, K. J. (2006). Ionospheric erosion by Alfvén waves. *J. Geophys. Res.*: *Space Phys.*, *111*(A3), A03206. https://doi.org/10.1029/2005JA011367

Chaston, C. C., Johnson, J. R., Wilber, M., Acuna, M., Goldstein, M. L., and Reme, H. (2009). Kinetic Alfvén wave turbulence and transport through a reconnection diffusion region. *Phys. Rev. Lett.*, *102*(1), 015001. https://doi.org/10.1103/PhysRevLett.102.015001

Chaston, C. C., Bonnell, J. W., Clausen, L., and Angelopoulos, V. (2012). Energy transport by kinetic-scale electromagnetic waves in fast plasma sheet flows. *J. Geophys. Res.*: *Space Phys.*, *117*(A09202). https://doi.org/10.1029/2012JA017863

Chaston, C. C., Bonnell, J. W., Wygant, J. R., Mozer, F., Bale, S. D., Kersten, K., Breneman, A. W., Kletzing, C. A., Kurth, W. S., … MacDonald, E. A. (2014). Observations of kinetic scale field line resonances. *Geophys. Res. Lett.*, *41*(2), 209–215. https://doi.org/10.1002/2013GL058507

Chen, C. X., and Wang, C. P. (2019). Contribution of patchy reconnection to the ion-to-electron temperature ratio in the Earth's magnetotail. *Earth Planet. Phys.*, *3*(6), 474–480. https://doi.org/10.26464/epp2019049

Chen, C. X. (2021). Preservation and variation of ion-to-electron temperature ratio in the plasma sheet in geo-magnetotail. *Earth Planet. Phys.*, *5*(4), 337–347. https://doi.org/10.26464/epp2021035

Chen, L., Wu, D. J., and Huang, J. (2013). Kinetic Alfvén wave instability driven by field-aligned currents in a low-β plasma. *J. Geophys. Res.*: *Space Phys.*, *118*(6), 2951–2957. https://doi.org/10.1002/jgra.50332

Cramer, N. F. (2001). *The Physics of Alfvén Waves*. Berlin: Wiley-VCH Verlag.

Dai, L. (2009). Collisionless magnetic reconnection via Alfvén eigenmodes. *Phys. Rev. Lett.*, *102*(24), 245003. https://doi.org/10.1103/PhysRevLett.102.245003

Dai, L., Wang, C., Zhang, Y. C., Lavraud, B., Burch, J., Pollock, C., and Torbert, R. B. (2017). Kinetic Alfvén wave explanation of the Hall fields in magnetic reconnection. *Geophys. Res. Lett.*, *44*(2), 634–640. https://doi.org/10.1002/2016GL071044

Dombeck, J., Cattell, C., Wygant, J. R., Keiling, A., and Scudder, J. (2005). Alfvén waves and Poynting flux observed simultaneously by Polar and FAST in the plasma sheet boundary layer. *J. Geophys. Res.*: *Space Phys.*, *110*(A12), A12S90. https://doi.org/10.1029/2005JA011269

Duan, S. P., Liu, Z. X., and Angelopoulos, V. (2012). Observations of kinetic Alfvén waves by THEMIS near a substorm onset. *Chin. Sci. Bull.*, *57*(12), 1429–1435. https://doi.org/10.1007/s11434-012-4973-x

Duan, S. P., Dai, L., Wang, C., Liang, J., Lui, A. T. Y., Chen, L. J., He, Z. H., Zhang, Y. C., and Angelopoulos, V. (2016). Evidence of kinetic Alfvén eigenmode in the near-earth magnetotail during substorm expansion phase. *J. Geophys. Res.*: *Space Phys.*, *121*(5), 4316–4330. https://doi.org/10.1002/2016JA022431

Duan, S. P., Dai, L., Wang, C., He, Z. H., Cai, C. L., Zhang, Y. C., Dandouras, I., Reme, H., André, M., and Khotyaintsev, Y. V. (2017). Oxygen ions O^+ energized by kinetic Alfvén eigenmode during dipolarizations of intense substorms. *J. Geophys. Res.*: *Space Phys.*, *122*(11), 11256–11273. https://doi.org/10.1002/2017JA024418

Ergun, R. E., Tucker, S., Westfall, J., Goodrich, K. A., Malaspina, D. M., Summers, D., Wallace, J., Karlsson, M., Mack, J., … Cully, C. M. (2016). The axial double probe and fields signal processing for the MMS mission. *Space Sci. Rev.*, *199*(1-4), 167–188. https://doi.org/10.1007/s11214-014-0115-x

Fu, H. S., Cao, J. B., Yang, B., and Lu, H. Y. (2011). Electron loss and acceleration during storm time: the contribution of wave–particle interaction, radial diffusion, and transport processes. *J. Geophys. Res.*: *Space Phys.*, *116*(A10), A10210. https://doi.org/10.1029/2011JA016672

Fu, H. S., Cao, J. B., Cully, C. M., Khotyaintsev, Y. V., Vaivads, A., Angelopoulos, V., Zong, Q. G., Santolík, O., Macúšová, E., … Zhima, Z. (2014). Whistler-mode waves inside flux pileup region: structured or unstructured?. *J. Geophy. Res.*: *Space Phys.*, *119*(11), 9089–9100. https://doi.org/10.1002/2014JA020204

Gary, S. P. (1986). Low-frequency waves in a high-beta collisionless plasma: polarization, compressibility and helicity. *J. Plasma Phys.*, *35*(3), 431–447. https://doi.org/10.1017/S0022377800011442

Gomberoff, L., and Elgueta, R. (1991). Resonant acceleration of alpha particles by ion cyclotron waves in the solar wind. *J. Geophys. Res.*: *Space Phys.*, *96*(A6), 9801–9804. https://doi.org/10.1029/91JA00613

He, J. S., Tu, C. Y., Marsch, E., and Yao, S. (2012a). Reproduction of the observed two-component magnetic helicity in solar wind turbulence by a superposition of parallel and oblique Alfvén waves. *Astrophys. J.*, *749*(1), 86. https://doi.org/10.1088/0004-637X/749/1/86

He, J. S., Tu, C. Y., Marsch, E., and Yao, S. (2012b). Do oblique Alfvén/ion-cyclotron or fast-mode/whistler waves dominate the dissipation of solar wind turbulence near the proton inertial length?. *Astrophys J.*, *745*(1), L8. https://doi.org/10.1088/2041-8205/745/1/L8

Hollweg, J. V. (1999). Kinetic Alfvén wave revisited. *J. Geophys. Res.*: *Space Phys.*, *104*(A7), 14811–14819. https://doi.org/10.1029/1998JA900132

Huang, H. T., Yu, Y. Q., Dai, L., and Wang, T. Y. (2018). Kinetic Alfvén waves excited in two-dimensional magnetic reconnection. *J. Geophys. Res.*: *Space Phys.*, *123*(8), 6655–6669. https://doi.org/10.1029/2017JA025071

Huang, S. Y., Yuan, Z. G., Ni, B., Zhou, M., Fu, H. S., Fu, S., Deng, X. H., Pang, Y., Li, H. M., … Yu, X. D. (2015). Observations of large-amplitude electromagnetic waves and associated wave–particle interactions at the dipolarization front in the earth's magnetotail: a case study. *J. Atmos. Sol. Terr. Phys.*, *129*, 119–127. https://doi.org/10.1016/j.jastp.2015.05.007

Huang, S. Y., Wei, Y. Y., Yuan, Z. G., Jiang, K., Deng, X. H., Xu, S. B., He, L. H., Zhang, J., and Zhang, Z. H. (2020). Electron jets in the terrestrial magnetotail: a statistical overview. *Astrophys. J.*, *896*(1), 67. https://doi.org/10.3847/1538-4357/ab8eb0

Keiling, A., Wygant, J. R., Cattell, C. A., Mozer, F. S., and Russell, C. T. (2003). The global morphology of wave Poynting flux: powering the aurora. *Science*, *299*(5605), 383–386. https://doi.org/10.1126/science.1080073

Keiling, A., Parks, G. K., Wygant, J. R., Dombeck, J., Mozer, F. S., Russell, C. T., Streltsov, A. V., and Lotko, W. (2005). Some properties of Alfvén waves: observations in the tail lobes and the plasma sheet boundary layer. *J. Geophys. Res.*: *Space Phys.*, *110*(A10), A10S11. https://doi.org/10.1029/2004JA010907

Keiling, A. (2009). Alfvén waves and their roles in the dynamics of the Earth's magnetotail: a review. *Space Sci. Rev.*, *142*(1-4), 73–156. https://doi.org/10.1007/s11214-008-9463-8

Kennel, C. F., and Petschek, H. E. (1966). Limit on stably trapped particle fluxes. *J. Geophys. Res.*, *71*(1), 1–28. https://doi.org/10.1029/JZ071i001p00001

Kletzing, C. A. (1994). Electron acceleration by kinetic Alfvén waves. *J. Geophys. Res.*: *Space Phys.*, *99*(A6), 11095–11103. https://doi.org/10.1029/94JA00345

Lindqvist, P. A., Olsson, G., Torbert, R. B., King, B., Granoff, M., Rau, D., Needell, G., Turco, S., Dors, I., … Tucker, S. (2016). The spin-plane double probe electric field instrument for MMS. *Space Sci. Rev.*, *199*(1-4), 137–165. https://doi.org/

10.1007/s11214-014-0116-9

Lysak, R. L., and Lotko, W. (1996). On the kinetic dispersion relation for shear Alfvén waves. *J. Geophys. Res.*: *Space Phys.*, *101*(A3), 5085–5094. https://doi.org/10.1029/95JA03712

Lysak, R. L. (1998). The relationship between electrostatic shocks and kinetic Alfvén waves. *Geophys. Res. Lett.*, *25*(12), 2089–2092. https://doi.org/10.1029/98GL00065

Moya, P. S., Pinto, V. A., Viñas, A. F., Sibeck, D. G., Kurth, W. S., Hospodarsky, G. B., and Wygant, J. R. (2015). Weak kinetic Alfvén waves turbulence during the 14 November 2012 geomagnetic storm: van Allen probes observations. *J. Geophys. Res.*: *Space Phys.*, *120*(7), 5504–5523. https://doi.org/10.1002/2014JA020281

Pollock, C., Moore, T., Jacques, A., Burch, J., Gliese, U., Saito, Y., Omoto, T., Avanov, L., Barrie, A., … Zeuch, M. (2016). Fast plasma investigation for magnetospheric multiscale. *Space Sci. Rev.*, *199*(1-4), 331–406. https://doi.org/10.1007/s11214-016-0245-4

Russell, C. T., Anderson, B. J., Baumjohann, W., Bromund, K. R., Dearborn, D., Fischer, D., Le, G., Leinweber, H. K., Leneman, D., … Richter, I. (2016). The magnetospheric multiscale magnetometers. *Space Sci. Rev.*, *199*(1-4), 189–256. https://doi.org/10.1007/s11214-014-0057-3

Sonnerup, B. U. Ö., and Scheible, M. (1998). Minimum and maximum variance analysis. *ISSI Scientific Reports Series*(1), 185–220.

Stasiewicz, K., Bellan, P., Chaston, C., Kletzing, C., Lysak, R., Maggs, J., Pokhotelov, O., Seyler, C., Shukla, P., … Wahlund, J. E. (2000). Small scale Alfvénic structure in the aurora. *Space Sci. Rev.*, *92*(3), 423–533. https://doi.org/10.1023/A:1005207202143

Voitenko, Y., and Goossens, M. (2006). Energization of plasma species by intermittent kinetic Alfvén waves. *Space Sci. Rev.*, *122*(1-4), 255–270. https://doi.org/10.1007/s11214-006-8212-0

Wahlund, J. E., Louarn, P., Chust, T., de Feraudy, H., Roux, A., Holback, B., Dovner, P. O., and Holmgre, G. (1994). On ion acoustic turbulence and the nonlinear evolution of kinetic Alfvén waves in aurora. *Geophys. Res. Lett.*, *21*(17), 1831–1834. https://doi.org/10.1029/94GL01289

Wang, X. Y., Huang, S. Y., Allen, R. C., Fu, H. S., Deng, X. H., Zhou, M., Burch, J. L., and Torbert, R. B. (2017). The occurrence and wave properties of EMIC waves observed by the Magnetospheric Multiscale (MMS) mission. *J. Geophys. Res.*: *Space Phys.*, *122*(8), 8228–8240. https://doi.org/10.1002/2017JA024237

Wygant, J. R., Keiling, A., Cattell, C. A., Lysak, R. L., Temerin, M., Mozer, F. S., Kletzing, C. A., Scudder, J. D., Streltsov, V., … Russell, C. T. (2002). Evidence for kinetic Alfvén waves and parallel electron energization at 4–6 R_E altitudes in the plasma sheet boundary layer. *J. Geophys. Res.*: *Space Phys.*, *107*(A8), 1201. https://doi.org/10.1029/2001JA900113

Young, D. T., Burch, J. L., Gomez, R. G., De Los Santos, A., Miller, G. P., Wilson IV, P., Paschalidis, N., Fuselier, S. A., Pickens, K., … Webster, J. M. (2016). Hot plasma composition analyzer for the magnetospheric multiscale mission. *Space Sci. Rev.*, *199*(1-4), 407–470. https://doi.org/10.1007/s11214-014-0119-6

Yuan, Z. G., Deng, X. H., Pang, Y., Li, S. Y., and Wang, J. F. (2007). Alfven waves in a plasma sheet boundary layer associated with near-tail magnetic reconnection. *Chin. Phys. Lett.*, *24*(4), 1122–1124. https://doi.org/10.1088/0256-307X/24/4/075